Singular Spectrum Analysis as a data-driven approach to the analysis of motor adaptation time series

Swart, Sander; den Otter, Rob; Lamoth, Claudine

Published in:
Biomedical signal processing and control

DOI:
10.1016/j.bspc.2021.103068

Publication date:
2022

Biomedical Signal Processing and Control 71 (2022) 103068

Contents lists available at ScienceDirect

Biomedical Signal Processing and Control

journal homepage: www.elsevier.com/locate/bspc

Singular Spectrum Analysis as a data-driven approach to the analysis of motor adaptation time series

S.B. Swart *, A.R. den Otter, C.J.C. Lamoth

University of Groningen, University Medical Centre Groningen, Department of Human Movement Sciences, Groningen, The Netherlands

ARTICLE INFO

Keywords:
Keywords: Adaptation
Motor learning
Singular Spectrum Analysis
split-belt

ABSTRACT

Motor adaptation is a form of learning to re-establish desired movements in novel situations. To probe motor adaptation, one can replicate such conditions experimentally by imposing a sustained perturbation during movement. Exposure to such perturbations initially causes an abrupt change in relevant performance variables, followed by a gradual return to baseline behaviour. The resulting time series exhibit persistent properties related to structural changes in underlying motor control and transitory properties related to trial-to-trial variations. The global trend, signifying the structural change, is often assessed by averaging the time series in predefined bins or nonlinear model fitting. However, these methods to study motor adaptation require *a priori* decisions to produce accurate fits. Here, we test a data-driven approach called Singular Spectrum Analysis (SSA) to assess the global trend. In SSA, we *first* decompose the adaptation time series into components that represent either a global trend or additional variations, and *secondly*, select the component(s) corresponding to the global trend using spectral analysis. In this paper, we will use simulated data to compare the reconstruction performance of SSA with often applied filter and fitting methods in motor adaptation studies and apply SSA to real data obtained during split-belt adaptation. In the simulations, we show that SSA reconstructed the fast-initial component and entire global trends more accurately than the filtering and fitting methods. In addition, we show that SSA also successfully reconstructed global trends from real data. Therefore, the SSA might be useful in motor learning studies to decompose and assess adaptation time series.

1. Background

Motor adaptation involves recalibrating a well-practiced motor task like walking to re-establish efficient task performance in response to altered environmental or task demands [1]. It is a form of motor learning that has been studied widely by imposing a sustained perturbation, like asymmetrical speeds during treadmill walking [2,3] and altered visual feedback during reaching [4]. Performance in these adaptation tasks is typically measured on a trial-to-trial basis as the difference between the perturbed and unperturbed movements during adaptation and baseline phases, respectively. Performance improvement is initially rapid but slows over time to an asymptote close to baseline performance levels [4,5]. This overall performance change results in an adaptation time series that exhibits persistent properties – the global adaptation trend related to structural changes in motor control – as well as transitory properties related to trial-to-trial variations (Fig. 1). In practice, the former is of interest for quantifying motor adaptation, while the transitory properties are usually considered a nuisance. To extract the global adaptation trend, adaptation time series are often averaged in predefined bins or fitted with nonlinear models [5–12]. However, these often applied methods to study motor adaptation necessitate *a priori* settings that make it difficult to achieve accurate fits for the idiosyncratic time series obtained from individual subjects. Here, we test the utility of Singular Spectrum Analysis (SSA) to discern the global adaptation trend from the transitory properties in a data-driven manner.

Both the persistent and transitory processes may contribute to motor adaptation. Consider for example a locomotor task in which participants walk on a split-belt treadmill. The velocity of the treadmill belts can be controlled independently and are set asymmetrically to elicit adaptation. During adaptation, the sensory prediction error – quantified as the difference between predicted and observed sensory feedback – will be large at first but will gradually decrease as learning proceeds. As a result, a persistent improvement in task performance occurs that reflects a structural recalibration in motor control for the remainder of the adaptation task. Besides the persistent improvement in task performance, adaptation time series also exhibit transitory properties. While

* Corresponding author.
E-mail address: s.b.swart@umcg.nl (S.B. Swart).

https://doi.org/10.1016/j.bspc.2021.103068
Received 5 May 2021; Received in revised form 18 July 2021; Accepted 8 August 2021
Available online 26 August 2021

such trial-to-trial variations may be random like noise, it might also represent an exploration of control possibilities within the imposed task demands that are relevant to the learning process [4,13]. Decomposing the adaptation time series into the persistent and transitory properties is thus necessary to probe the different aspects of motor control more transparently.

In motor control studies, filtering and fitting methods are often applied to signals that represent adaptation or learning processes to identify its persistent properties. Such filtering methods typically include moving- and bin-average filters, in which the data across the adaptation time series are averaged in a bin that is time-shifted by a lag of 1 data point or a lag equal to the bin size [5–8]. These methods act as low-pass filters that attenuate the transitory variations in the time series. Increasing the bin size will attenuate larger transitory variations more effectively but can shift the filtered time series in phase. Hence, the effectiveness of filtering methods depends on both the spectral content of a time series and the *a priori* choice of the bin-size. As the former can differ between participants, bin sizes are chosen quite arbitrarily. In addition to filtering, fitting methods are also applied to assess the global adaptation trend. Since adaptation generally follows an exponential pattern, single- or double exponential have been fitted to (averaged) adaptation time series [9–12]. The fit is typically evaluated based on the goodness of fit index R^2 - which reflects how much of the variance in the data is explained by the fit. Yet, justifying the choice for a single or double exponential based on this index may be spurious, as R^2 is considered an inadequate measure for such nonlinear models [14]. In addition, fitting methods also require *a priori* estimates of the floating parameters in the model. Results of algorithms to fit nonlinear models based on gradient descent, like the Levenberg–Marquardt, are sensitive to such initial parameter estimates [15]. Overall, the above issues underscore the necessity of an approach capable of discerning the global adaptation trend from transitory properties accurately without needing *a priori* settings.

Here we test the application of SSA [16,17]. SSA is a data-driven and non-parametric approach that can be used to extract a global trend from a given time series, even in the presence of transitory properties that cannot be specified *a priori*. SSA decomposes the original time series into components that represent the global trend and components that represent additional variations (e.g., local trends or seasonality) or noise. Since the global adaptation trend and transitory properties occur on different time scales [18] and span a largely separable frequency domain [13], spectral analysis can identify the component(s) that reflect the global trend in a time series. In this paper, we test the utility of SSA as a data-driven approach for deconstructing adaptation time series by (**i**) giving a description of the SSA algorithm, (**ii**) comparing the global trend reconstruction between SSA and often applied filter and fitting methods in motor adaptation studies with simulated data, (**iii**) illustrating the utility of SSA for computing the rate of change in motor adaptation, and (**iv**) illustrating the use of the SSA method on real data obtained during split-belt adaptation.

2. Description of the standard SSA algorithm

Figs. 2–4 illustrate the steps in the standard SSA algorithm. To

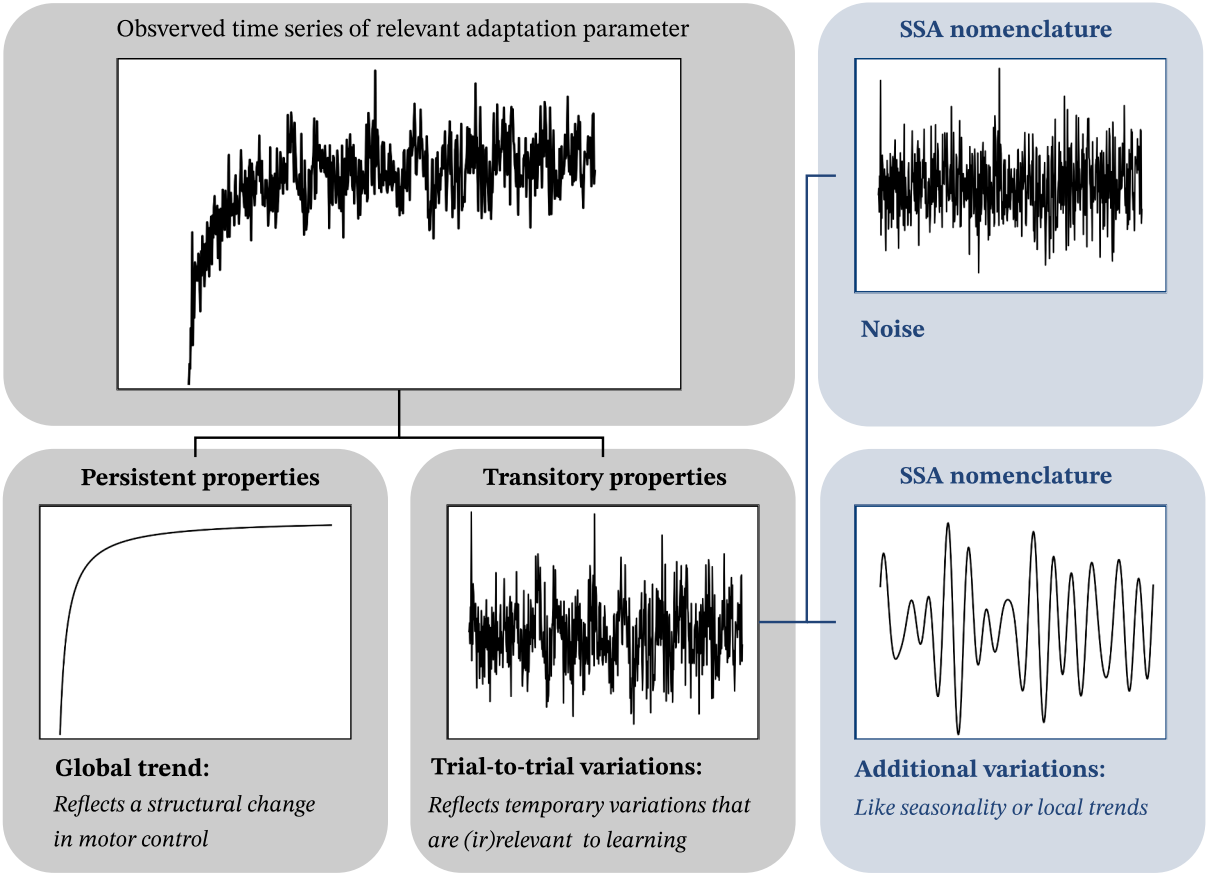

Fig. 1. Conceptual signal. Left upper panel shows an observed time series of a relevant adaptation parameter. This adaptation time series exhibits persistent and transitory properties. The former is defined as the global adaptation trend which reflects the structural change in motor control. Transitory properties form the residuals and reflect trial-to-trial variations that appear random but may still contain relevant aspects of the adaptation process, such as exploratory behaviour that supports more structural changes in motor control. In Singular Spectrum Analysis (SSA) nomenclature (blue), the transitory properties are often subdivided and termed additional variations, such as seasonality or local trends, and noise.

explain these steps, we simulated an adaptation-like time series Y_N as a positive, monotonic function asymptotic to 0.

$$Y_N = -1 + \frac{N}{a+N} + \sigma \quad 0 \leqslant N < 600$$

The decay rate a of the global trend $-1+N/(a+N)$ was set to 10, and the error term σ was normally distributed white noise with a signal-to-noise ratio of 0.5. SSA will be applied here to reconstruct the global trend $-1+N/(a+N)$ from Y_N.

An overview of the first step in SSA is provided in Fig. 2. Step 1 represents the embedding procedure of the SSA. Here, Y_N is decomposed into lagged vectors (lag = 1) to construct the so-called trajectory matrix $\mathbf{X}$ (Fig. 2). Each lagged vector is transposed and embedded as a column of the trajectory matrix $\mathbf{X}$. The result is an $L \times K$ trajectory matrix with a Hankel structure, as the elements along the diagonal are equal. Window length L, representing the embedding dimension, has to be specified by the user, whereas column length K is defined as $K = N - L + 1$. The value of L has to be reasonably large such that each lagged vector incorporates an essential part of the time series' behaviour but not larger than $N/2$ [16,19,20]. In practice, it is advisable to check the result for different values of L as minor adjustments may improve the separability between the components. Based on previous studies [16,19,20], we use a window length $L = \lfloor N/2 \rfloor$ here, where $\lfloor . \rfloor$ denotes a floor function and N denotes the series length.

In the second step, we compute the (unstandardized) principal component vectors (PVs). The trajectory matrix $\mathbf{X}$ is first multiplied by its transpose to compute a square $L \times L$ matrix $\mathbf{S} = \mathbf{X}\mathbf{X}^\top$. Next, the eigendecomposition of matrix $\mathbf{S}$ is obtained by:

$$\mathbf{S} = \mathbf{E}\Lambda\mathbf{E}^\top \tag{1}$$

which results in an orthogonal matrix $\mathbf{E}$ of eigenvectors, a diagonal matrix Λ of eigenvalues, and an orthogonal matrix $\mathbf{E}^\top$ of transposed eigenvectors. The eigenvalues λ are arranged in descending order of their magnitudes ($\lambda_1 \geqslant \lambda_2 \geqslant \ldots \geqslant \lambda_L \geqslant 0$). Multiplying the transposed trajectory matrix $\mathbf{X}^\top$ by the orthogonal matrix $\mathbf{E}$ of eigenvectors yields the PVs of matrix $\mathbf{S}$ as columns of matrix $\mathbf{A}$:

$$\mathbf{A} = \mathbf{X}^\top\mathbf{E} \tag{2}$$

In SSA, the global trend is reconstructed through the addition of a number of selected, slow-varying components. Figs. 3 and 4a, b illustrate the steps to identify these global trend components. Spectral analysis of the PVs is used to discern the global trend and residual components [21]. The set of PVs reflecting the global trend are the components that represent low-frequency time series (Fig. 4c1-2), whereas PVs reflecting the residuals represent high-frequency time series (Fig. 4c3). Hence the global trend components can be identified automatically by assessing the low-frequency contribution $\mathscr{C} \in [0,1]$ of individual PVs in a low-frequency domain (Fig. 3b). This domain is specified by $\omega_0 \in (0, 0.5)$ – a low-frequency boundary that can be inferred from Y_N's periodogram by assessing the last index larger than its median (Fig. 3a) [21]. Importantly, the ω_0 governs the scale of the extracted trend, i.e., a lower boundary will result in a slower varying trend, while a higher boundary will result in a more oscillatory trend. Therefore, the ω_0 can have a substantial impact on the overall reconstruction performance of the SSA and should be reported in the analysis of empirical adaptation data.

The low-frequency contribution $\mathscr{C}$ of each PV is computed by summing its periodogram in the low-frequency domain (Fig. 3b). The low-frequency domain is $[0, (\lceil K\omega_0 \rceil / K)]$ here as the difference between length N of Y and K of the PV causes different resolution of their periodograms. Candidate trend components will have a relatively large contribution, whereas candidate residual components will have a relatively small contribution $\mathscr{C}$ in this low-frequency domain.

Global trend components are identified by computing an optimal low-frequency threshold $\{\mathscr{C}_0 | \mathscr{C}_0 \in \{0.50, 0.51, \ldots, 1\}\}$ iteratively (Fig. 4a, b). A global trend is reconstructed for each $\mathscr{C}_0$ by summing the reconstructed components (RC) of PVs with a low-frequency contribution $\mathscr{C}$ higher than the $\mathscr{C}_0$ value. Reconstruction is achieved by multiplying PVs (stored as columns in matrix $\mathbf{A}$) by $\mathbf{E}^\top$ and subsequently averaging the skew diagonals of the resultant matrix (Fig. 4d). Since global trend components have a higher contribution in the low-frequency domain, the normalized residual low-frequency contribution will be lower when these components are in the reconstructed trend (Fig. 4a). Increasing the threshold precludes more components from the preliminary trends, and hence, the normalized residual low-frequency contribution becomes higher when the contribution threshold $\mathscr{C}_0$ increases. Assessing the point where the differentiated residual low-frequency contribution increases above threshold $\mathscr{R} \in [0.05, 0.1]$ gives rise to the optimal $\mathscr{C}_0^{\mathscr{R}}$ value (Fig. 4b) [21].

In the final step, the identified components are summed to reconstruct the global trend, and the remaining components are summed to reconstruct the residuals (Fig. 4e).

2.1. Modifications of the standard SSA algorithm for motor adaptation time series

The global trend of time series is assumed to be slowly varying in the standard SSA algorithm. However, trends in adaptation data typically start with a steep curve since the vast majority of learning occurs early in the adaptation process. In this case, we found that the standard SSA algorithm often failed to reconstruct the time series' initial steepness accurately. We addressed this issue by using an overlap (OV) SSA [22], in which the standard SSA is applied separately to consecutive,

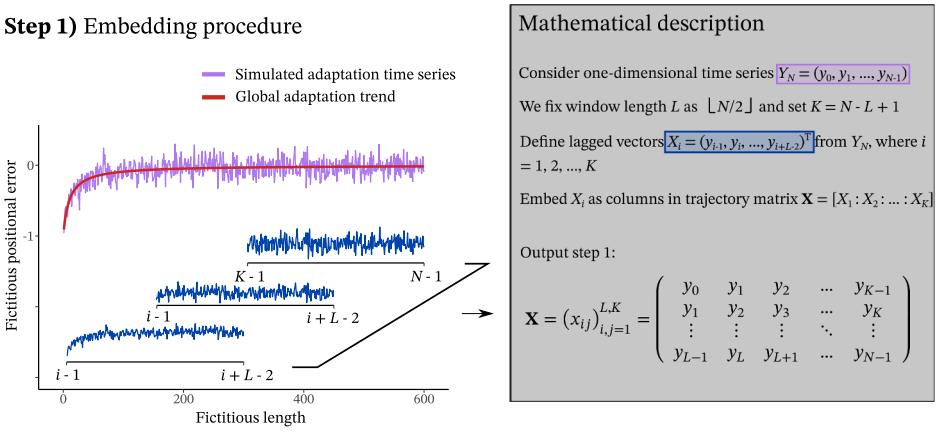

Fig. 2. Step 1 in Singular Spectrum Analysis (SSA). The time series (purple) is decomposed into lagged vectors (blue). Each lagged vector is transposed and embedded as a column in the so-called trajectory matrix $\mathbf{X}$.

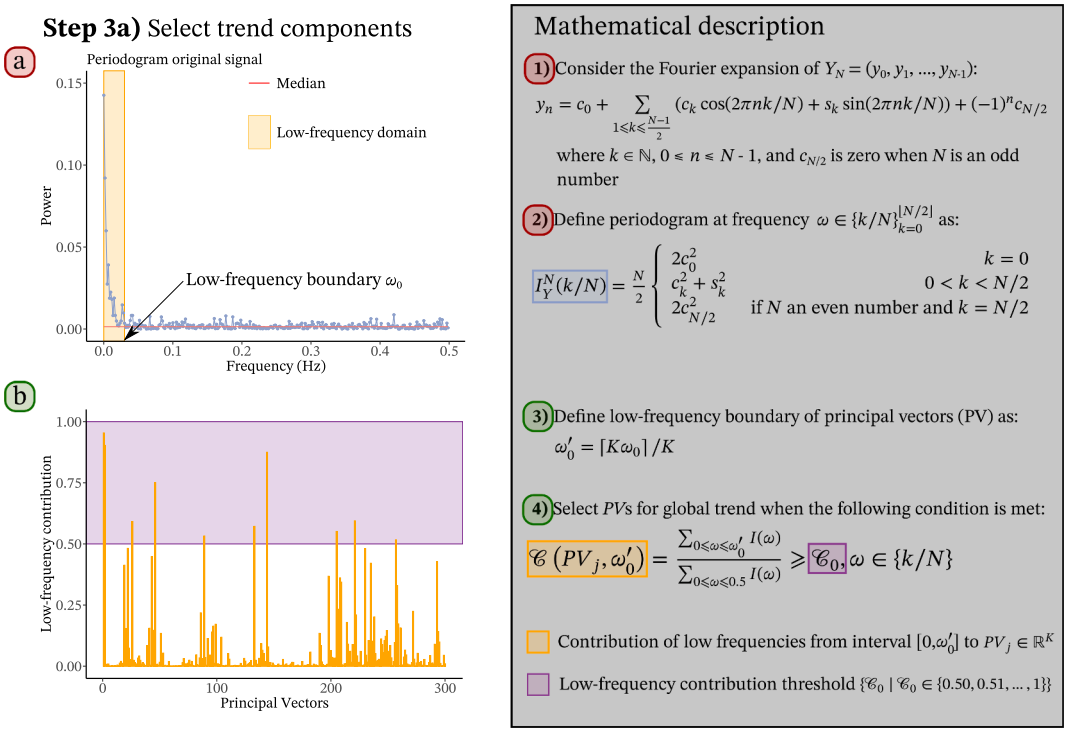

Fig. 3. First steps in Singular Spectrum Analysis (SSA) to identify the global trend components. **a)** Compute the periodogram of the original time series to infer a low-frequency boundary ω_0. **b)** Adjust the low-frequency boundary for the principal vectors (PVs) and compute the low-frequency contribution of each PV. The purple block represents the domain in which the low-frequency threshold $\mathscr{C}_0$ is searched. This procedure is illustrated in Fig. 4.

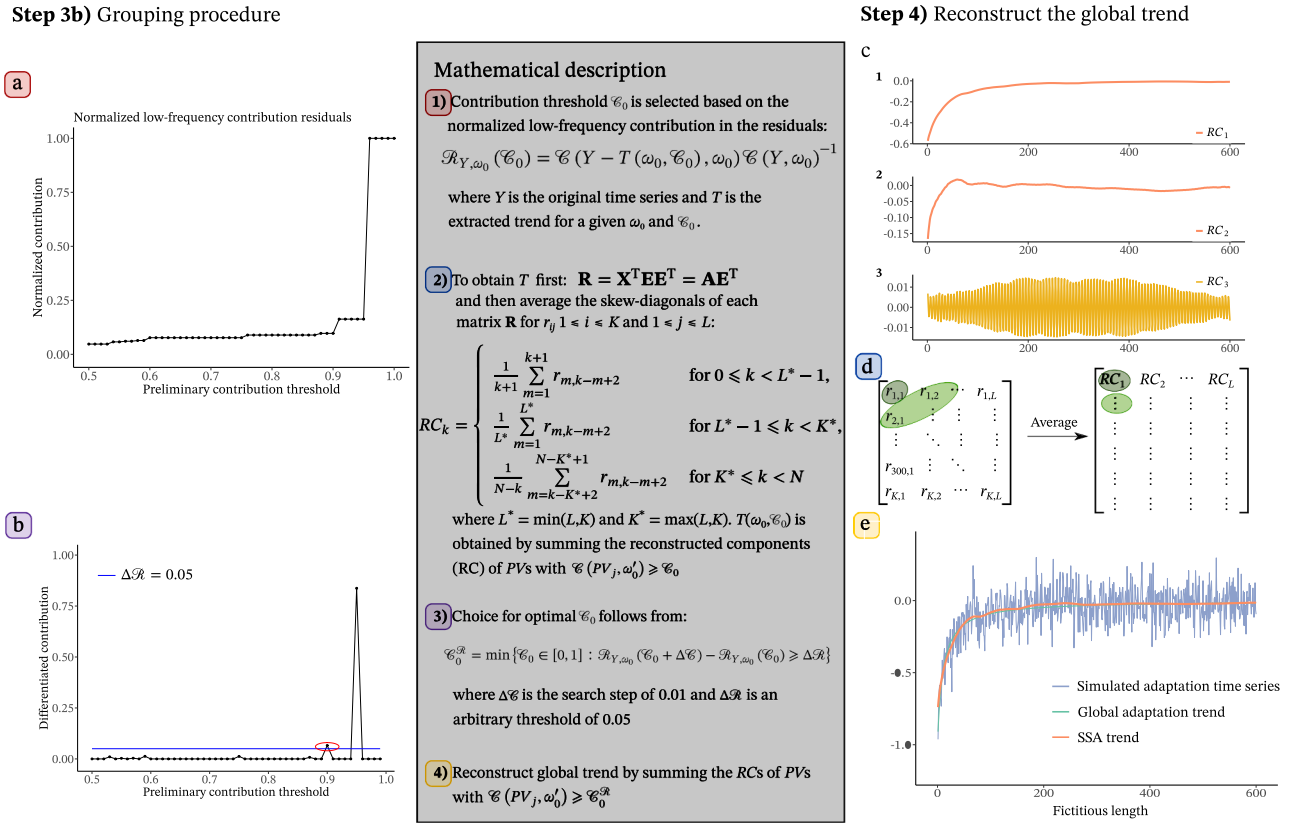

Fig. 4. Complement steps in Singular Spectrum Analysis to identify the global trend components. **a)** To identify the optimal low-frequency contribution threshold $\mathscr{C}_0$, we first compute the normalized low-frequency contribution in the residuals for different values of $\mathscr{C}_0$ (x-axis). **b)** The point where the differentiated low-frequency contribution in the residuals increases above 0.05 gives rise to the optimal threshold. **c)** Examples of reconstructed components (RC), $RC_{1,2}$ were identified as trend components. **d)** Diagonal averaging procedure for obtaining the RCs. **e)** Final result of the SSA which is obtained by summing $RC_{1,2}$.

overlapping segments with the same length. Since the spectral analysis that we used in the grouping step can be computational costly and requires time series with sufficient length, we only used two overlapping segments for the adaptation time series. That is, for a given time series $Y_N = (y_0, y_1, \ldots, y_{N-1})$, we apply the standard SSA on $(y_0, \ldots, y_{Z-1})$ and $(y_q, \ldots, y_{N-1})$. At the end of the first and beginning of the second segment, $(Z-q)/2$ data points are discarded to reduce the artifacts at the intersection of the two segments. A global trend is reconstructed within each segment, which are then merged to acquire the full reconstruction of the time series' global trend. This procedure could improve the reconstruction of the time series' initial steepness, paramount for analysing motor adaptation time series.

3. Simulation examples

With simulated data, we compared the performance of SSA with fitting- and filtering methods in reconstructing global trends. The simulated time series were chosen on the premise that an adaptation time series is constituted by a global adaptation trend and transitory variations. A global trend was defined as a monotonic series asymptotic to 0 and was simulated as $-1 + N/(a+N)$. This global trend resembles the typical time course of motor adaptation, with its decay rate defined by a. We contaminated this global trend by adding transitory variations as the sum of 3 (co)sine waves, with varying amplitudes A and periods φ, and zero-mean white noise σ. That resulted in adaptation-like time series A_N:

$$A_N = -1 + \tfrac{N}{a+N} + \left(A_1\cos\left(\tfrac{2\pi N}{\varphi_1}\right) + A_2\sin\left(\tfrac{2\pi N}{\varphi_2}\right) + A_3\sin\left(\tfrac{2\pi N}{\varphi_3}\right)\right) + \sigma$$

With $0 \leqslant N < 600$

Simulations were used to test how accurately the different methods could reconstruct the global trend $-1 + N/(a+N)$ from A_N in the presence of transitory properties. In the supplementary, a similar simulation is provided for a double exponential adaptation time series to test the different methods for a more complex shaped curve.

3.1. Simulation procedures

The simulations were performed 100 times in custom-made MATLAB (version r2016b; The Mathworks Inc., Natick, MA) routines. At each simulation, the decay rate $a \sim U[5, 20]$, the amplitudes $A_{1,2,3} \sim U[0.01, 0.05]$, the periods $\varphi_1 \sim U[30, 40]$, $\varphi_2 \sim U[40, 50]$, $\varphi_3 \sim U[60, 70]$ and the white noise $\sigma \sim U[0.25, 5]$ were drawn from a uniform distribution U so that each value within the boundaries was equally likely to occur. The boundaries for these distributions were chosen arbitrarily to ensure that the simulated time series approximated empirical adaptation time series. In each simulation, the standard SSA and OV-SSA were used to extract the global trend. For comparison, we also used commonly employed filtering and fitting methods to extract the global trend. These included a moving-average filter, a bin-average filter, and a curve-fitting procedure.

Based on methods used in previous studies, the bin size was set to 3 for the moving-average filter [5,8], and 5 for the bin-average filter [6]. Since we simulated a monotonic, exponential time series, curve-fitting was done with a single exponential model and 3-floating parameters in the form of $y = a * \exp^{-N/b} + c$ [9,10,12]. Bounds (lower, starting point, upper) on the a (-5, −1, 0), b (0, 5, Inf.), and c (-Inf., 0, Inf.) parameters were specified *a priori* and estimated with the Levenberg–Marquardt algorithm. For the standard SSA and OV-SSA, the window length L was fixed as $\lfloor N/2 \rfloor$. Since we wanted to improve the reconstruction of the time series' initial steepness with the OV-SSA, the first segment length Z was set to 60 data points – the period in which the initial steepness approximately occurs - and q was set to 2. The length of segment Z should be sufficiently long to ensure that the trend and residuals components can be accurately separated. Based on our own experience, we recommend to keep the length of the first segment between ∼ 8% and ∼ 16% of N. For the first and the second overlapping segment, we defined the low-frequency boundary ω_0 as the first local minimum between the peaks generated by the global trend and transitory variations in the periodogram of A_N. This method to estimate the low-frequency boundary ω_0 was used for the standard SSA as well. Since the simulated series have a known global trend $-1 + N/(a+N)$, we can assess the trend reconstruction performance for the different methods by computing the root mean squared error (RMSE) between the actual and reconstructed global trend for the entire series' length and specifically for the initial 60 data points, given its significance for motor adaptation analysis.

3.2. Application of SSA for computing adaptation parameters

In addition to the trend reconstruction, we illustrate the applicability of SSA for computing relevant adaptation parameters. For that, we used the rate of change – a parameter that signifies a fraction of the total adaptive change in the performance parameter. We quantified this as the summed rate of change in adaptation during the first minute relative to the total adaptation:

$$Rate\ of\ change = \frac{\sum_{1}^{60}(Y_N)'}{\sum_{1}^{N}(Y_N)'} \tag{3}$$

in which the numerator represents the absolute rate of change in the first minute, Y represents a reconstructed trend and N represents the length of Y.

The rates of change were computed for the reconstructed trends of the OV-SSA, standard SSA, curve-fitting, bin- and moving-average filters. To assess the performance, we computed relative rates of change by subtracting the rate of change of each method from the true rate of change based on the simulated global trends. Values above zero would indicate an underestimation, whereas values below zero would indicate an overestimation of the true rate of change. As the true rate of change depends on the decay rate a of the simulated global trend, we assessed whether this influenced the performance of each method by grouping its rate of change based on A_N's decay rate as slow $a \in [16, 20]$, medium $a \in [11, 15]$, and fast $a \in [5, 10]$.

3.3. Reconstruction performance for the different methods

Fig. 5 and Table 1 show the trend reconstruction results. For the entire adaptation time series, the OV-SSA and curve-fitting resulted in the smallest RMSE between the actual and reconstructed global trend (Fig. 5a; Table 1). Standard SSA performed slightly less accurately (Fig. 5a), which was presumably caused by an inaccurate reconstruction of the time series' initial segment (Fig. 5b, g). RMSEs were highest for the bin- and moving-average filters (Fig. 5a; Table 1), mainly because the transitory variations were not filtered out entirely (Fig. 5e-f). Apart from the standard SSA, bin- and moving-average filters were also the least accurate in reconstructing the initial segment (Fig. 5b). Curve-fitting and the OV-SSA performed slightly better in reconstructing the initial segment (Fig. 5b).

3.4. The accuracy of different methods in quantifying the rate of change

Table 2 and Fig. 6 show the relative rates of changes for the different methods. Estimating the rate of change with bin- or moving-average filtered time series yielded on average similar rates as the true rates but with a considerably higher spread (Table 2; Fig. 6). The performance of filtering was not markedly different for the slow, medium, and fast decay rates of the simulated global trends (Table 2). Both curve-fitting and standard SSA performed better, given the lower spread in rates (Fig. 6) – although the standard SSA underestimated the true rate. In addition, curve-fitting performed slightly worse for slow compared to

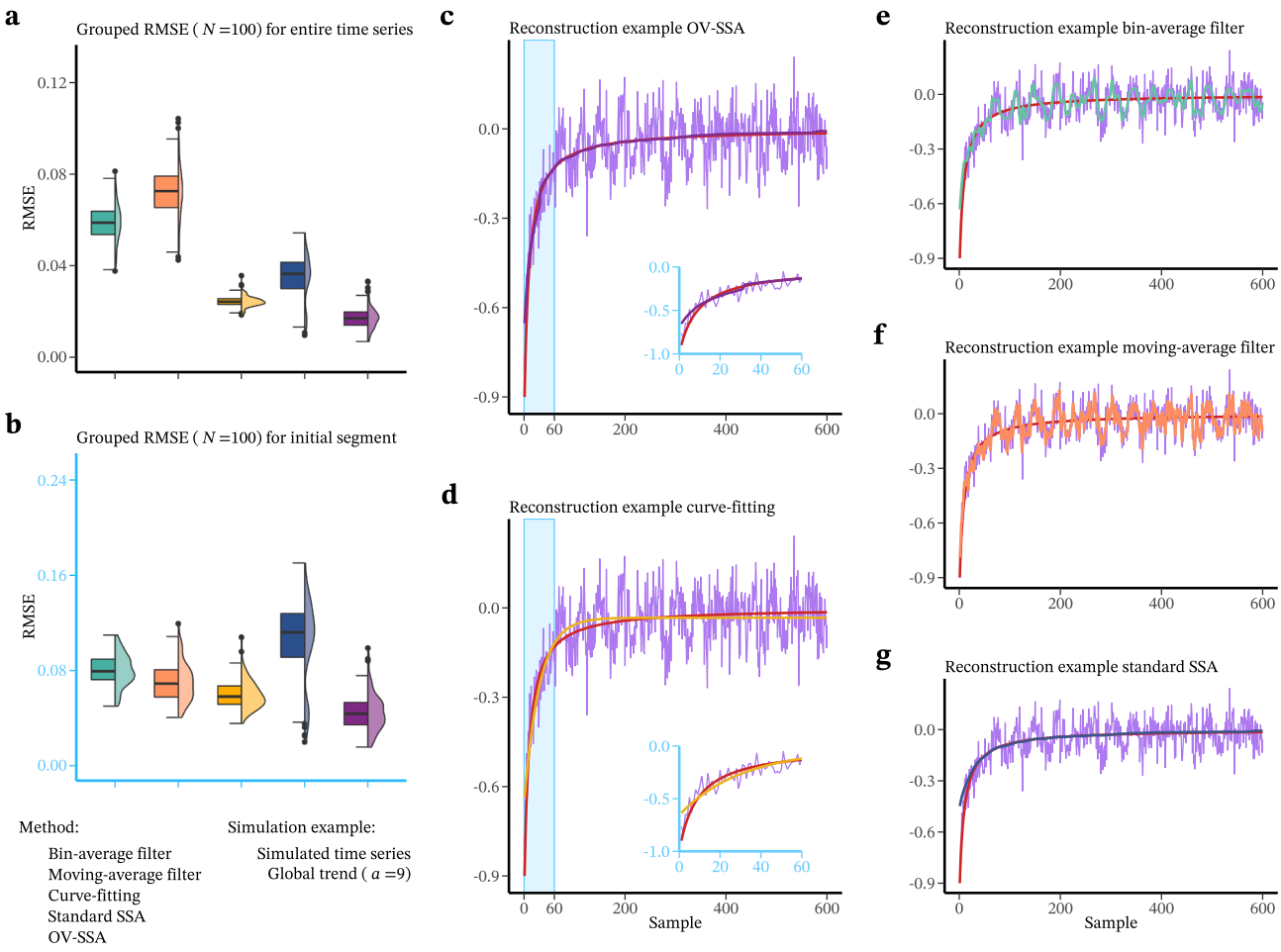

Fig. 5. Trend reconstruction. **a)** Root mean squared errors (RMSE) ($N = 100$) for the entire adaptation time series between the actual and reconstructed trends for bin-averaging (green), moving-averaging (orange), curve-fitting (yellow), standard Singular Spectrum Analysis (SSA) (blue), and overlap (OV)-SSA (purple). **b)** RMSE ($N = 100$) results for the initial segment from 1–60 (cyan). **c-d)** Examples of OV-SSA (purple) and curve-fitting (yellow) in reconstructing the global trend (red, decay rate $a = 9$) of a simulated adaptation time series A_N (light purple). Zoom on the initial segment is provided in cyan. **e-g)** Examples of bin-averaging (green), moving averaging (orange), and standard SSA (blue) in reconstructing the global trend.

Table 1
Descriptive statistics for the trend reconstruction. Root mean squared errors (RMSE) between actual and reconstructed trends.

	Method				
	Bin-average	Moving-average	Curve fitting	Standard SSA	OV-SSA
Entire time series					
Mean ± std (N = 100)	0.059 ± 0.009	0.072 ± 0.013	0.025 ± 0.003	0.034 ± 0.011	0.017 ± 0.005
Initial segment*					
Mean ± std (N = 100)	0.081 ± 0.014	0.070 ± 0.016	0.060 ± 0.012	0.102 ± 0.037	0.045 ± 0.016

*The initial segment is defined as the first 60 data points.

faster decay rates (Table 2). The OV-SSA performed well in estimating the rate of change across the different decay rates (Table 2; Fig. 6).

4. Application of SSA to real adaptation data

As shown in the simulations, SSA performs accurately in reconstructing trends from the exponential adaptation time series. Yet, in practice, individual adaptation time series can also have atypical shapes.

Table 2
Descriptive statistics for the rate of change in adaptation. For each method, rates of change were computed and subtracted from the true rate of change based on the simulated global trend (total). In addition, these relative rates of change were grouped based on the decay rate a of the simulated curve (slow, medium, and fast).

Method	Rates of change (Mean ± std)			
	Total (N = 100)	Slow* (N = 38)	Medium** (N = 30)	Fast***(N = 32)
Bin-average	0.010 ± 0.114	0.003 ± 0.110	-0.022 ± 0.117	0.047 ± 0.110
Moving-average	0.000 ± 0.132	0.018 ± 0.155	-0.046 ± 0.126	0.021 ± 0.096
Curve-fitting	0.042 ± 0.054	0.074 ± 0.044	0.039 ± 0.044	0.006 ± 0.050
Standard SSA	0.141 ± 0.069	0.150 ± 0.072	0.127 ± 0.075	0.142 ± 0.059
OV-SSA	0.048 ± 0.036	0.057 ± 0.035	0.043 ± 0.037	0.042 ± 0.034

*Decay rates simulated asymptotes between 16 and 20.
**Decay rates simulated asymptotes between 11 and 15.
***Decay rates simulated asymptotes between 5 and 10

Therefore, we also illustrate the performance of SSA on time series collected during split-belt adaptation. In response to the split-belt configuration (i.e., asymmetrical belt speeds), subjects initially walk

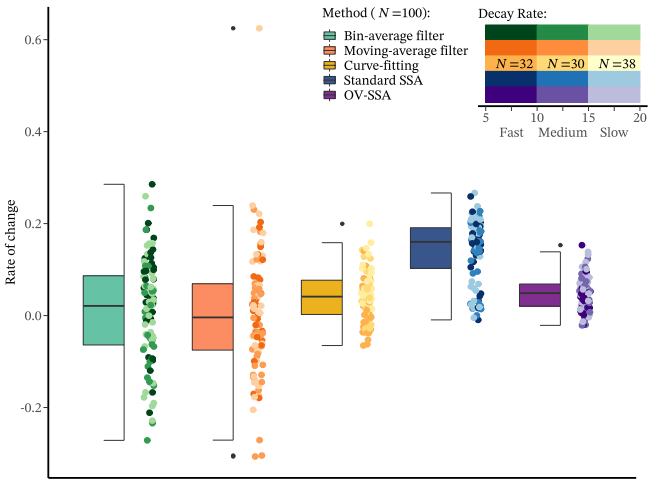

Fig. 6. Rate of change in adaptation. Box plots show the relative rate of change ($N = 100$) for each method. These included the bin-average filter (green), moving-average filter (orange), curve-fitting (yellow), standard Singular Spectrum Analysis (SSA) (blue), and overlap (OV)-SSA (purple). Scatter plots show the relative rate of change for fast, medium, and slow decay rates a of the simulated global trends. Darker colours reflect rates of change for fast decay rates between 5 and 10 ($N = 32$), slightly lighter colours reflect medium decay rates between 11 and 15 ($N = 30$), and the lightest colours reflect slow decay rates between 16 and 20 ($N = 38$).

asymmetrically, but they adapt their step lengths towards symmetry over the course of the adaptation phase. The ratio between the left and right step lengths (i.e., the step length symmetry) is typically derived as a measure of adaptation [2]. To illustrate the applicability of SSA for trend extraction in real data, we used step length symmetry series from a previously published study in our lab (see for details: [3,23]).

The step length symmetry was calculated for every step i as follows [2]:

$$Step\ length\ symmetry(i) = \frac{Step\ length\ left(i) - Step\ length\ right(i)}{Step\ length\ left(i) + Step\ length\ right(i)} \tag{4}$$

where the step length was defined as the difference in fore aft centre of pressure position at heel strike. Step length symmetry series from 3 participants were used to extract a global adaptation trend with OV-SSA and curve-fitting. The filter methods were precluded for this part because those had the least accurate performance in the simulations. Settings for the OV-SSA were the same as in the simulations. For comparison, we fitted both a single and double exponential $y = a * \exp^{-N/b} + c * \exp^{-N/d}$ to the data using the Levenberg–Marquardt algorithm. Single exponential was fitted with parameter bounds a (-1, −0.8, 0), b (0, 5, Inf.) and c (-Inf., 1, Inf.), whereas the double exponential was fitted with parameters bounds a (-1, −0.8, 0), b (0, 2, Inf.), c (-Inf., 1, Inf.) and d (0, 2, Inf.). Visual inspection of the residuals was used to analyse the adequacy of the fit. Since the global trend is slowly varying, the residuals should have a low contribution in the low-frequency domain when the fit is accurate. We quantified this contribution LF as follows:

$$LF = \frac{\sum_{0 \leqslant \omega \leqslant 0.2} I(\omega)}{\sum_{0 \leqslant \omega \leqslant 0.5} I(\omega)}, \quad \omega \in \{k/N\} \tag{5}$$

where values closer to 1 indicate a higher low-frequency contribution in the residuals. Besides the periodograms, we also provided QQ-plots of the residuals as these have been used previously to analyse the adequacy of the fit [24]. Deviation of normality (i.e., deviation from $y = x$) indicates either that the trend reconstruction was not accurate or that the residuals have a different structure than zero-mean white noise.

Fig. 7 shows three real examples of split-belt adaptation. The first example is a step length symmetry series with a typical exponential shape (Fig. 7a). In this example, both the single- and double exponentials (LFs = 0.492) provide decent fits of the data, which is to be expected as the general shape of the adaptation time series is exponential (Fig. 7a–c). The OV-SSA provides a decent fit for this adaptation series as well ($LF = 0.469$) but is not restricted to monotonicity (i.e., a function persevering order) like the single-exponential fit. This effect is more evident in the third example, in which the step length symmetry series has an atypical shape (Fig. 7g). Here, the single exponential cannot capture the initial decrease of the adaptation time series ($LF = 0.739$). The double exponential can capture this initial decrease but strongly underfits the second half of adaptation (i.e., between 300 and 574) ($LF = 0.726$). For this atypical adaptation time series, the OV-SSA provides the best fit as it accurately captures the global adaptation trend, and its residuals have a lower contribution of low-frequencies (Fig. 7g-i) ($LF = 0.656$). Similar results are observed for a different atypical adaptation time series (Fig. 7d). Both the single- ($LF = 0.691$) and double ($LF = 0.656$) exponentials overfit the data around 150 and show a relatively high contribution of lower frequencies (Fig. 7d-f). In contrast, the OV-SSA captures the atypical shape accurately as its residuals have a small contribution of lower frequencies ($LF = 0.626$). Overall, compared with curve-fitting, the OV-SSA captures global adaptation trends more accurately for atypical adaptation time series.

5. Discussion

Adaptation is a long-standing paradigm used in motor learning studies [1]. These studies yield adaptation time series that reflect the overall learning performance. The global adaptation trend related to structural changes in control can be difficult to infer as subjects show large intersubject variability in adaptation time series. Here, we tested the utility of SSA to assess the global adaptation trend from (a)typical adaptation time series. For typically shaped adaptation time series, we showed with simulations that SSA reconstructed the global adaptation trends more accurately than the filtering and fitting methods that are often employed in motor control studies. Furthermore, we illustrated with real data that SSA reconstructed global adaptation trends from atypically shaped adaptation time series more accurately than curve-fitting procedures. Collectively, the results showed that SSA might be useful in motor learning studies to isolate the global trends from the overall learning performance.

Accurately assessing the global adaptation trend is a prerequisite to quantify aspects of the adaptation process (e.g., rate of change). In the simulations, we demonstrated that the OV-SSA reconstructed the global adaptation trends more accurately than the included filtering and fitting methods. As a result, estimates of the rate of change were also more accurate for OV-SSA extracted trends than for filtered or fitted trends. In addition, the accuracy of estimated rates of change with the OV-SSA was consistent across the different decay rates of the simulated adaptation time series. In practice, the use of SSA might thus result in more accurate detection of relevant adaptation parameters. This is evidenced further by the fact that SSA reconstructed the global trends from the split-belt adaptation time series more accurately than curve-fitting. Overall, we showed that the often applied filter and fitting methods to study motor adaptation quantified the global trend less accurate than SSA, which concomitantly affected the computed adaptation aspects.

The initial segment of the adaptation time series is an important, but difficult to quantify, aspect of motor learning. In the simulations, we showed that the OV-SSA reconstructed the initial segment more accurately than the bin- and moving-average filters. A disadvantage of these filtering methods is that its performance depends on the spectral characteristics of a time series. Therefore, high frequencies in the simulated time series, such as transient fluctuations, could not be effectively attenuated with filtering. Curve-fitting was only slightly less accurate than SSA in the simulations presumably because the exponential model was in accordance with the shape and monotonicity of the simulated

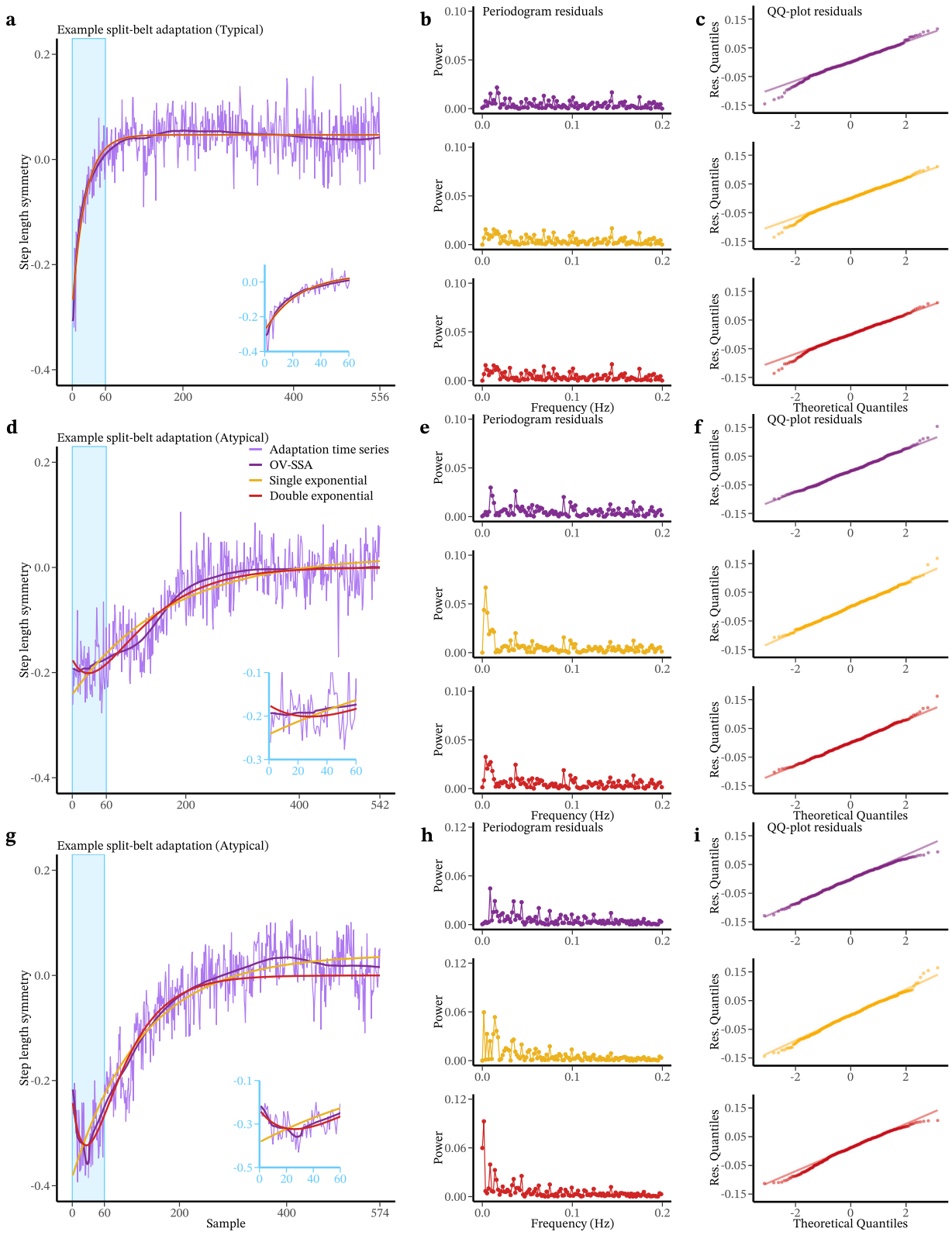

Fig. 7. Trend extraction split-belt data. **a, d, g)** Three global trend reconstruction examples of step length symmetry (light purple) using the overlap-Singular Spectrum Analysis (OV-SSA) (dark purple), single exponential (yellow) and double exponential fit (red). **b, e, h)** Shows the periodogram of the residuals – accurate extraction of slow-varying trend should be reflected in a low contribution for low-frequencies in the residuals. **(c, f, i)** Shows QQ-plots of the residuals – deviation of normality indicates either inaccurate trend reconstruction or residuals having a different structure than zero-mean white noise.

adaptation time series. Indeed, for split-belt adaptation time series with an atypical shape during initial adaptation, single-exponential models underfitted the atypical shape (e.g., see Fig 7d, g). Taken together, we demonstrated with simulations that SSA reconstructed the fast-initial component of adaptation slightly more accurately than filter and fitting methods. Relative to these methods, SSA might perform considerately more accurate in practice given the limitations of these filter and fitting methods to produce accurate fits for idiosyncratic time series.

While SSA is thus suited for non-parametric reconstruction of global trends, with model-based approaches, like curve-fitting, one can formalize and test hypotheses about adaptation. Single- and dual-rate state-space models have been used to explain certain adaptation phenomena, like the ability to recall previously made adaptations when re-exposed to the same adaptation task (i.e., savings) [10]. For instance, it has been shown that split-belt adaptation involves two processes that operate at different rates – a process with a fast learning rate but weak retention and a process with a slow learning rate but strong retention [10]. Formalizing and testing such hypotheses with SSA are unsuited because this approach is data-driven. In addition to formalizing hypotheses, Rashid and colleagues (2020) [24] recently addressed the issues with initial parameter guesses and measures for the adequacy of the fit in nonlinear regression. Their propositions might improve the fit of a nonlinear model for (double) exponential adaptation time series [24]. Then, only the model's assumption about the shape of the global trend remains.

Yet, changes in the performance over time may reveal trends that cannot be described properly by an exponential time course (e.g., see split-belt examples). Then, the analysis should not make *a priori* assumptions about the shape of the global trend. A data-driven approach, like SSA, makes it possible to map individual adaptation processes and to identify potential subpopulations based on this. SSA is quite flexible in this sense because it allows the reconstruction of various frequency bands by adjusting the parameters in the grouping step. Quantifying subtle changes in learning performance (more) accurately may provide further insights into the mechanisms that underly ageing and pathology. Furthermore, it is important to achieve an adequate decomposition of the time series to detect the trial-to-trial variations accurately. Recently, it was found that trial-to-trial variations may represent the exploration of control solutions that facilitates motor learning [13]. Although the residuals were not analysed in this paper, assessing to what extent these are still partly deterministic or merely noise irrelevant to the adaptation process could provide further insights into healthy and pathological motor control.

While we considered SSA, various other detrending methods, such as empirical mode decomposition (EMD) and wavelet transform, are available as well. EMD has often been used in the decomposition of electroencephalographic (EEG) signals prior to detecting synchrony [25] because it does not need arbitrary bandpass filter cut-offs, like the Fourier Transform, and works well for nonstationary signals [26]. One of EMD's drawbacks, however, concerns its end-effect problem [26]. While in EEG data, this can be resolved by recording before and after the period of interest [25], such an approach is not feasible within a motor adaptation paradigm. Unlike SSA and EMD that are fully driven by the time series itself, wavelet transforms decompose time series in the time/frequency domain. Although wavelets are suitable to detect events on short time scales, such as sit-to-stand or stand-to-sit transitions in a Timed-Up-and-Go test [27], or gait events [28], SSA is more suitable for examining motor adaptation which takes place both on the short- and long-time scale. Furthermore, in the wavelet transform, a mother wavelet has to be selected *a priori* as a basis function. All told, the SSA is not the only available or best method overall for detrending, but it is able to reconstruct fast initial component of learning and does not require many parameter settings *a priori*.

To summarize, the SSA outlined in this tutorial is suited to quantify global trends from nonstationary[1] adaptation and washout time series. SSA extracted these global trends more accurately than often applied filtering and fitting methods in motor control studies. Given its accurate performance and flexibility, SSA might be beneficial for various research topics in human movement sciences that deal with heterogeneous time series. Quantifying persistent (or more fluctuating) properties therein might further enhance our understanding of human movement and control.

Funding

This research did not receive any specific grant from funding agencies in the public, commercial, or not-for-profit sectors

CRediT authorship contribution statement

S.B. Swart: Conceptualization, Methodology, Formal analysis, Writing – original draft, Visualization. **A.R. den Otter:** Conceptualization, Methodology, Writing – review & editing. **C.J.C. Lamoth:** Conceptualization, Methodology, Writing – review & editing.

Declaration of Competing Interest

The authors declare that they have no known competing financial interests or personal relationships that could have appeared to influence the work reported in this paper.

Appendix A. Supplementary data

Supplementary data associated with this article can be found, in the online version, at https://doi.org/10.1016/j.bspc.2021.103068.

References

[1] J.W. Krakauer, A.M. Hadjiosif, J. Xu, A.L. Wong, A.M. Haith, Motor Learning, Compr. Physiol. 9 (2019) 613–663.
[2] Darcy S. Reisman, Hannah J. Block, Amy J. Bastian, Interlimb coordination during locomotion: what can be adapted and stored? J. Neurophysiol. 94 (2005) 2403–2415.
[3] D. Vervoort, et al., Do gait and muscle activation patterns change at middle-age during split-belt adaptation? J. Biomech. 99 (2020), 109510.
[4] J.A. Taylor, J.W. Krakauer, R.B. Ivry, Explicit and implicit contributions to learning in a sensorimotor adaptation task, J. Neurosci. 34 (2014) 3023–3032.
[5] L.A. Malone, A.J. Bastian, Thinking about walking: effects of conscious correction versus distraction on locomotor adaptation, J. Neurophysiol. 103 (2010) 1954–1962.
[6] L.A. Malone, A.J. Bastian, Age-related forgetting in locomotor adaptation, Neurobiol. Learn. Mem. 128 (2016) 1–6.
[7] C. Rossi, et al., The capacity to learn new motor and perceptual calibrations develops concurrently in childhood, Sci. Rep. 9 (2019) 9322–9326.
[8] T. Honda, M. Hirashima, D. Nozaki, Adaptation to visual feedback delay influences visuomotor learning, PLoS One 7 (2012), e37900.
[9] L.A. Malone, E.V. Vasudevan, A.J. Bastian, Motor adaptation training for faster relearning, J. Neurosci. 31 (2011) 15136–15143.
[10] F. Mawase, L. Shmuelof, S. Bar-Haim, A. Karniel, Savings in locomotor adaptation explained by changes in learning parameters following initial adaptation, J. Neurophysiol. 111 (2014) 1444–1454.
[11] R.C. Miall, N. Jenkinson, K. Kulkarni, Adaptation to rotated visual feedback: a re-examination of motor interference, Exp. Brain Res. 154 (2004) 201–210.
[12] J. Fernandez-Ruiz, W. Wong, I.T. Armstrong, J.R. Flanagan, Relation between reaction time and reach errors during visuomotor adaptation, Behav. Brain Res. 219 (2011) 8–14.
[13] H.G. Wu, Y.R. Miyamoto, L.N. Gonzalez Castro, B.P. Ölveczky, M.A. Smith, Temporal structure of motor variability is dynamically regulated and predicts motor learning ability, Nat. Neurosci. 17 (2014) 312–321.
[14] A.N. Spiess, N. Neumeyer, An evaluation of R2 as an inadequate measure for nonlinear models in pharmacological and biochemical research: a Monte Carlo approach, BMC Pharmacol. 10 (2010), 6–6.

[1] For time series with linear-like tendencies, is it recommended to (double) centring the data or to use a so-called Toeplitz SSA approach [16].

[15] H.P. Gavin, The Levenberg-Marquardt algorithm for nonlinear least squares curve-fitting problems, in: Department of Civil and Environmental Engineering, 28, Duke University, 2011, pp. 1–5.
[16] N. Golyandina, V. Nekrutkin, A. Zhigljavsky, Analysis of Time Series Structure: SSA and Related Techniques, Chapman & Hall/CRC, New York, 2001.
[17] D.S. Broomhead, G.P. King, Extracting qualitative dynamics from experimental data, Physica D 20 (1986) 217–236.
[18] K.M. Newell, Y.T. Liu, G. Mayer-Kress, Time scales in motor learning and development, Psychol. Rev. 108 (2001) 57–82.
[19] N. Golyandina, On the choice of parameters in Singular Spectrum Analysis and related subspace-based methods, Stat. Interface 3 (2010) 259–279.
[20] H. Hassani, R. Mahmoudvand, M. Zokaei, Separability and window length in singular spectrum analysis, Comptes Rendus Mathematique 349 (2011) 987–990.
[21] T.A. Alexandrov, Method of Trend Extraction Using Singular Spectrum Analysis, Revstat Stat. J. 7 (2009) 1–22.
[22] M.C.R. Leles, J.P.H. Sansão, L.A. Mozelli, H.N. Guimarães, A new algorithm in singular spectrum analysis framework: The Overlap-SSA (ov-SSA), SoftwareX 8 (2018) 26–32.
[23] D. Vervoort, et al., Adaptive control of dynamic balance across the adult lifespan, Med. Sci. Sports Exerc. 52 (2020) 2270–2277.
[24] U. Rashid, N. Kumari, N. Signal, D. Taylor, A.C. Vandal, On nonlinear regression for trends in split-belt treadmill training, Brain Sci. 10 (2020) 737.
[25] C.M. Sweeney-Reed, S.J. Nasuto, A novel approach to the detection of synchronisation in EEG based on empirical mode decomposition, J. Comput. Neurosci. 23 (1) (2007) 79–111.
[26] N. Huang, Z. Shen, S. Long, M. Wu, H. Shih, Q. Zheng, N.-C. Yen, C. Tung, H. Liu, The empirical mode decomposition and the Hilbert spectrum for nonlinear and non-stationary time series analysis, Proc. R. Soc. Lond. 454 (1998) 903–995.
[27] D. Vervoort, N. Vuillerme, N. Kosse, T. Hortobágyi, C.J. Lamoth, Multivariate analyses and classification of inertial sensor data to identify aging effects on the timed-up-and-go test, PLoS One 11 (6) (2016).
[28] P.M. Forsman, E.M. Toppila, E.O. Haeggstrom, Wavelet analysis to detect gait events, Annu. Int. Conf. IEEE Eng. Med. Biol. Soc. (2009) 424–427.